
On the definition of the flow width for calculating specific catchment area patterns from gridded elevation data

Giovanni Battista Chirico,^{1*} Andrew W. Western,² Rodger B. Grayson²
and Günter Blöschl³

¹ *Department of Agriculture Engineering, Università di Napoli 'Federico II', Via Università, 100-80055 Portici (NA), Italy*

² *Centre for Environmental Applied Hydrology and Cooperative Research Centre for Catchment Hydrology, Department of Civil and Environmental Engineering, University of Melbourne, Melbourne, Australia*

³ *Institut für Hydraulik, Gewässerkunde und Wasserwirtschaft, Technische Universität Wien, Wien, Germany*

Abstract:

Specific catchment area (SCA) patterns are commonly computed on grids using flow direction algorithms that treat the flow as coming from a point source at the pixel centre. These algorithms are all ambiguous in the definition of the flow width to be associated with a pixel when computing the SCA. Different methods for computing the flow width have been suggested, without giving an objective reason. In the few cases where this issue has been specifically discussed, the flow width is derived from subjective analysis and incorrect conceptualizations. This paper evaluates alternative approaches for defining the flow width when computing SCA patterns using the D_{∞} and D8 algorithms, by comparing theoretical and computed SCA patterns on sloping planes, inward and outward cones. Two new methods of defining the flow width are also analysed for both the D_{∞} and D8 algorithms. The performances of the different methods are discussed in relation to two dimensionless parameters: (1) the global resolution, defined as the ratio of a characteristic length of the study area to the grid size and (2) the upslope area resolution, defined as the ratio of the theoretical SCA to the grid size. The optimal methods are identified by specific threshold values of these dimensionless parameters. We conclude that assuming the flow width invariant and equal to the grid size is generally the best approach in most practical circumstances, both for the D_{∞} and D8 algorithm. Copyright © 2005 John Wiley & Sons, Ltd.

KEY WORDS distributed modelling; digital terrain analysis; specific catchment area; flow direction algorithms; flow width

INTRODUCTION

The specific catchment area (SCA) is defined as the total upslope catchment plan area (TCA) draining across a unit length of contour (Moore *et al.*, 1991). SCA is an estimate of the local lateral discharge rate under the following three hypotheses: (1) uniform upslope recharge rate; (2) equilibrium condition of the upslope catchment response (steady-state assumption); and (3) lateral flow (either subsurface or surface flow) parallel to the surface slope and therefore perpendicular to the unit contour length defining the unit flow width. SCA can also be interpreted as a characteristic length or extent of the upslope catchment area for the processes controlling the lateral response of the catchment.

SCA patterns, combined with other variables, such as other terrain attributes or soil–vegetation properties, are commonly used in hydrological and geomorphological applications. For example, SCA is used to predict patterns of relative saturation (e.g., Beven and Kirkby, 1979; O’Loughlin, 1981), the spatial occurrence of shallow landslides (e.g., Montgomery and Dietrich, 1994) and patterns of erosion thresholds (e.g., Dietrich *et al.*, 1993).

* Correspondence to: Giovanni Battista Chirico, Dipartimento di Ingegneria Agraria, Via Università, 100-80055 Portici (NA), Italy.
E-mail: gchirico@unina.it

Received 16 September 2003

Accepted 16 July 2004

SCA patterns are computed by analysis of the terrain with different methods. Among these, grid-based procedures are the most popular. In this paper we critically discuss the definition of the flow width when computing the SCA on grids, focusing in particular on the D ∞ and D8 algorithms. We evaluate different approaches for computing the flow widths by comparing the computed SCA patterns with theoretical ones for simple geometries, such as a sloping plane, an outward cone and an inward cone. These are similar to those used by Costa-Cabral and Burges (1994) and Tarboton (1997) for testing their terrain analysis algorithms. We also introduce and evaluate new approaches for computing the flow widths when using the D ∞ and D8 algorithms. These methods are derived by analysing the properties of the computed upslope catchment area patterns and flow direction on sloping planes.

The analysis on the simple geometries is carried out by considering two dimensionless parameters: (1) the global resolution, defined as the ratio of a characteristic length of the study area (defined below) to the grid size and (2) the upslope area resolution, defined as the ratio of the theoretical SCA to the grid size. The first is used to describe the average error statistics across the entire area for different grid sizes. The second is used to describe the patterns of relative error associated with different grid sizes.

The need for the second index stems from the fact that the error of the computed SCA in a pixel is related partly to the approximations of the algorithm applied and partly to the quality of the grid representation of the upslope area. Therefore the performance of different algorithms in terms of relative error has to be analysed by comparing the values of pixels with similar upslope area resolution, as the errors in pixels with similar upslope area resolution are likely to be more evenly affected by the quality of the gridded representation of the upslope area.

METHODS FOR COMPUTING SCA PATTERNS ON GRIDS: A BRIEF REVIEW

In general, prior to the computation of a SCA pattern, a preliminary terrain analysis is done to produce an intermediate data set that includes: (1) the spatial discretization of the terrain in a network of elemental units (element network); (2) the connectivity among the elements; and (3) the element terrain attributes. The spatial discretization is generally related to the method used to structure the elevation data and to the spacing of the elevation data. The element connectivity defines how the elemental units are laterally connected. In particular, for each element, the connectivity defines: (1) the downslope elements and (2) the proportion of outgoing lateral fluxes allocated to each downslope element. The terrain attributes define the attributes of the elements that are relevant to the description of the lateral flow and of some vertical processes. Elements are generally assumed planar with a trapezoidal shape. Thus the element attributes are computed by averaging in space the three-dimensional properties of the element. Examples of element attributes are the spatial dimensions of the element, the slope and orientation of the flow within the element, which normally also defines the element aspect.

It is normally preferable to keep this terrain analysis as a separate computational step, so that the corresponding data set can be used consistently in other terrain-based hydrological applications requiring information in addition to the SCA pattern.

Procedures based on grids or on triangulated irregular networks (TINs) require little effort in the spatial discretization, as they produce a network structured according to the spatial distribution of the point elevation data. On the other hand, these procedures are more demanding in the computation of the element connectivity and attributes, as it is necessary to overcome inconsistencies between the element network structure and the underlying hypotheses concerning the lateral flow direction.

In contrast, contour-based procedures require more effort in the construction of the element network, by partitioning the terrain using contours and flow lines orthogonal to the contours. The resulting network geometry is structured according to the lateral slope, making the computation of the connectivity and terrain attributes straightforward (Moore *et al.*, 1991) and the computation of the SCA patterns more faithful to the SCA definition.

Contour-based methods are not robust, however, because the construction of the element networks is complicated, time-consuming and error-prone. Catchments containing complex terrain often need extensive user intervention, with fine-tuning and addition and deletion of contours in order to avoid invalid flow lines (Maunder, 1999). Contour-based networks are also an inefficient structure for creating and storing spatial data. For all these reasons, contour-based networks are not commonly used in hydrological applications.

Overall, grid-based procedures are the most popular, for practical rather than for physical reasons. They are also preferred to TIN-based methods, because the irregularity of TINs makes the computation of element connectivity and attributes more difficult (Moore *et al.*, 1991) and because spatial regularity is preferred for practical aspects related to the management of spatial data.

There are a variety of algorithms for calculating specific catchment area for gridded data, but they are conceptually similar (except for DEMON) and we first outline the general approach. All the methods first calculate a contributing area for each cell. Figure 1 illustrates the process of calculating the contributing area for the D8 single direction algorithm. The small numbers in the lower left of each cell show the elevation and the solid lines and arrows show the element connectivity, which is determined by finding the steepest descent direction in this algorithm. To calculate the contributing area at the downstream boundary of a given cell it is then a matter of summing up all the cells that (have the potential to) contribute flow across the downstream boundary. The larger numbers in the upper right corners show the contributing area determined using the D8 algorithm. To calculate the specific contributing area, these numbers are then divided by a representative flow width, the calculation of which is the main topic of this paper. In the case of multi-direction flow algorithms (e.g., Tarboton, 1997, see below), the connectivity is defined differently as shown for the cell labelled 'A' by the heavy dashed lines. In this case a proportion of the contributing area of cell 'A' is assigned to each of cells 'B' and 'C'. The proportions and number of downslope cells vary depending on exactly which algorithm is used, however, SCA is again obtained by summing the upslope area contributing to each cell and dividing by the representative flow width.

Different algorithms have been proposed to analyse gridded elevation data. These algorithms can be distinguished in two main categories: single-flow-direction (sfd) algorithms and multiple-flow-direction (mfd) algorithms. Sfd algorithms connect each element with a single downslope element. Mfd algorithms connect each element with one or more downslope elements. In the latter case, the proportion of outgoing flow allocated to each downslope element is part of the definition of the connectivity.

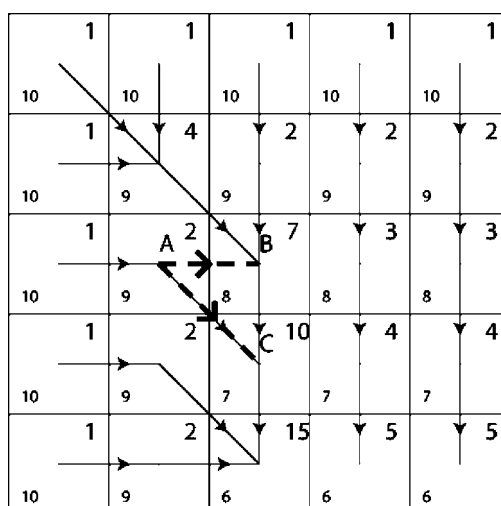


Figure 1. Schematic description concerning the computation of SCA patterns on gridded elevation data. The small numbers in the lower left of each cell show the elevation. The larger numbers in the upper right of each cell show the upslope area determined using the D8 algorithm. The solid lines and arrows show the element connectivity

Sfd algorithms include D8 (O'Callaghan and Mark, 1984), Rho8 (Fairfield and Leymarie, 1991) and Lea's method (Lea, 1992). Mfd methods include those proposed by Quinn *et al.* (1991) and Freeman (1991), hereafter referred to as MS methods (Multiple directions based on Slope) as in Tarboton (1997), and $D\infty$ (Tarboton, 1997).

All these algorithms produce a discretization of the terrain in rectangular pixels, the sizes of which are defined by the spacing of the elevation data. The centre of the pixel is considered as a point source of the outgoing lateral flow and the flow is treated as one-dimensional. For a given pixel, the sum of its area and the upslope area contributing to it is distributed among the surrounding downslope elements.

The methods differ in the criteria adopted in the definition of the downslope elements and the proportions of the outgoing flow to be accredited to each of the downslope elements. Basically these criteria arise from different approaches followed in defining the local slopes and flow directions on the basis of the relative differences in elevation between a pixel and its eight surrounding pixels.

Mfd algorithms have generally been recognized as performing better than sfd algorithms, at least at the hillslope scale. MS methods are used in nearly all hydrological applications based on the TOPMODEL approach (e.g., Quinn *et al.*, 1995). $D\infty$ has been shown to give the best results in defining the lateral flow directions and in resolving patterns of upslope contributing area (Tarboton, 1997).

Among the sfd methods, D8 is still generally used due to its ease of implementation. D8 is also recommended for representing the flow direction in the channel areas, where mfd algorithms can produce unrealistic dispersion of the upslope area patterns (Gallant and Wilson, 2000).

Both single- and multiple-flow direction methods are ambiguous in the definition of the flow width to be associated with each pixel according to the flow direction. This uncertainty comes from treating the flow as one-dimensional (Costa-Cabral and Burges, 1994). The same flow direction algorithm has been applied with different approaches in the definition of the flow width, without giving an objective reason. When explicitly discussed, the flow width has been defined by projecting the rectangular pixel or part of it to the orthogonal of the computed flow direction. Although this approach may appear 'physically based', it arises from an incorrect conceptualization in that it considers the flow to be two-dimensional, whereas the flow direction has been computed by assuming one-dimensional flow.

Quinn *et al.* (1991) explicitly defined the contour length (effectively flow width) to be associated with each pixel according to different flow directions in their MS method, and they used the contour length itself as weight factor in the computation of the proportion of flow allocated to each downslope element. They obtained the contour length by projecting a half pixel in the corresponding flow direction. However, while presenting their method, they clearly stated that this was 'subjectively chosen' and 'other choices are clearly possible'. Wolock and McCabe (1995), using other subjective arguments, proposed slightly different values of contour lengths to be associated with each pixel when they applied Quinn *et al.*'s (1991) MS method.

Also, two different methods have been used in the literature for computing the flow width in association with D8, without explanation for the chosen method. In some applications the flow width is assumed equal to the grid size (e.g., Zhang and Montgomery, 1994; Wolock and McCabe, 1995). In other applications the flow width is assumed equal to the grid size only when flow is oriented in a cardinal direction, while it is equal to the length of the pixel diagonal when it is oriented along a diagonal direction, as the pixel diagonal is equal to the projection of the pixel in the diagonal direction (e.g., Costa-Cabral and Burges, 1994; Gallant and Wilson, 2000).

No methods have been explicitly discussed for the computation of the flow width in association with $D\infty$. In the few known applications, the flow width is assumed equal to the grid size independently of the flow direction (e.g., Pack *et al.*, 1998).

It is worth noting that the minimum and maximum values suggested for flow width on gridded DEMs are 0.354 (e.g., Quinn *et al.*, 1991) and 1.414 times the pixel size (e.g., Costa-Cabral and Burges, 1994; Gallant and Wilson, 2000), respectively, both of which are suggested for the diagonal flow orientation. The flow width may not be a real issue when distribution models, such as TOPMODEL (e.g., Quinn *et al.*, 1995), are used to compute the global response of the catchment, as in this case only the statistics of the spatial

patterns of SCA are employed and these are not significantly affected by the range of flow widths that can be reasonably chosen (Quinn *et al.*, 1995). However, it may be more relevant when spatial patterns of SCA are used to predict spatial patterns of hydrologic and geomorphologic characteristics. In fact, differences between the maximum and minimum flow width values suggested in the literature can cause variation in SCA values of a factor of 4.

Costa-Cabral and Burges (1994) recognized the limitations of previous approaches in treating the flow as one-dimensional and suggested a new procedure called DEMON, which is an excellent alternative. DEMON is quite different from the other algorithms suggested for computing SCA on gridded elevation data. It is the only procedure we know of where the terrain analysis is not part of an intermediate step, rather it is 'in-built' in the algorithm applied for the computation of the SCA. DEMON in fact does not produce an element network.

DEMON treats the flow originating from each pixel as two-dimensional and defines a polygon representing the upslope area by tracing flow lines upslope from two corners of each pixel. It also objectively and correctly defines the flow width to be associated with each pixel, by projecting the pixel to the orthogonal of the flow direction. Essentially, DEMON disaggregates each element into a number of elements equal to the number of flow tubes crossing the elements. Therefore, it does not assign the proportions of outflow to each downslope pixel unequivocally, i.e., the connectivity among the pixels.

Ultimately, DEMON is the most precise algorithm for resolving the SCA patterns on grids, however, as with the contour-based methods, it is not robust and cannot be used in all practical circumstances (Tarboton, 1997). For this reason and because it does not produce an explicit grid network, single- and multiple-flow-direction algorithms are generally preferred in practical applications.

In the following sections we discuss the computation of SCA patterns with D_{∞} and D8 algorithms, testing the results on simple geometries: a planar slope, an inward cone and an outward cone.

PLANAR SLOPES

Here we discuss the definition of the pixel flow width for D_{∞} and D8, by comparing theoretical and computed patterns on planar slopes. Figure 2 shows a planar slope discretized in square pixels. The cross-hatched pixels define the downslope boundary of the analysed slope. L is the characteristic spatial dimension in the y direction and it represents the extent of the plane upslope of the marked pixels; d is the grid size, i.e. the spacing of the elevation data. The ratio $\rho = L/d$ defines the resolution of the grid in representing the sloping plane relative to the cross-hatched pixels. In this section ρ will be called the 'plane resolution'. The plane has infinite length in the x direction. The direction of the slope is defined by the angle α with the y direction; α ranges between 0 and $\pi/4$ radians.

The theoretical SCA at the centre of a pixel located at a distance l from the top edge of the slope is:

$$a_T = \frac{l}{\cos \alpha} = d \frac{2\mu - 1}{2 \cos \alpha} \quad (1)$$

where μ is the resolution of the plane relative to the pixel of interest; $\mu = \rho$ for the pixels located at the toe of the slope analysed in Figure 2.

The corresponding upslope catchment area resolution is:

$$\lambda(\mu, \alpha) = \frac{a_T}{d} = \frac{2\mu - 1}{2 \cos \alpha} \quad (2)$$

Next we compare these theoretical values to those computed using the D_{∞} and D8 algorithms.

Planar slope— D_{∞}

D_{∞} computes the SCA patterns after defining the local flow direction. The local flow direction is a continuous quantity and is equal to the direction of the steepest downward slope among eight triangular facets

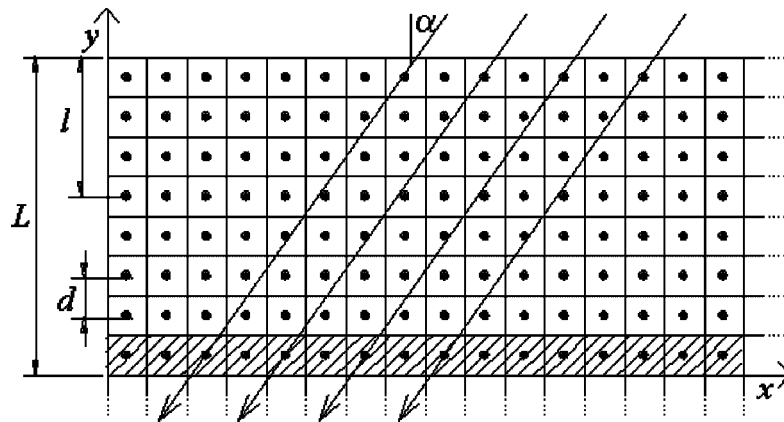


Figure 2. Planar slope, flow direction and characteristic dimensions

formed in a 3×3 pixel window centred on the pixel of interest (Tarboton, 1997). Each of these triangular facets has a downward slope vector starting from the pixel centre. The vector can lie within or outside the 45° angle of the facet at the pixel centre. If the slope vector is within this angle, it represents the steepest flow direction on that facet. If the slope vector angle is outside the facet, the steepest flow direction associated with that facet is taken along the steepest edge. The magnitude and direction of the steepest downslope vector from all eight facets are taken as the slope and flow direction of the grid pixel. The D_∞ procedure searches for the facet with the largest slope, proceeding anticlockwise from the east direction. The outgoing flow is then allocated to one or two downslope elements in the cardinal and/or diagonal directions, proportionally to the respective separating angles from the steepest descent vector (Tarboton, 1997).

In the specific case of the planar slope, D_∞ computes the flow direction correctly as the steepest descent vector is oriented according to the actual steepest direction along the plane. The total contributing area (TCA) computed by D_∞ at the centre of a pixel located at a distance l from the top edge of the slope is equal to $(l + 0.5)d$. Assuming the flow width equal to the grid size d independently from the flow direction, as in past applications of the D_∞ algorithm (e.g., Pack *et al.*, 1998), the computed specific catchment area is:

$$a_C = \frac{(l + 0.5)d}{d} = \mu d \quad (3)$$

We call this approach $D_\infty d$. The bias between computed and theoretical SCA on a strip of pixels along the direction y is a function of the plane resolution and the slope direction:

$$\text{BIAS}_{D_\infty d}(\rho, \alpha) = \frac{\sum_{\mu=1}^{\rho} (a_C - a_T)}{\rho} = \frac{L}{2\rho \cos \alpha} [1 - (1 + \rho)(1 - \cos \alpha)] \quad (4)$$

If plane resolution is progressively increased, the bias does not converge asymptotically to zero, unless α is zero:

$$\rho \rightarrow \infty, \text{BIAS}_{D_\infty d}(\rho, \alpha) \rightarrow -L \frac{1 - \cos \alpha}{2 \cos \alpha} \quad (5)$$

The local relative error can be expressed as a function of the upslope area resolution and the flow direction:

$$\text{LRE}_{D_\infty d}(\lambda, \alpha) = \frac{a_C - a_T}{a_T} = \frac{1}{2\lambda} - (1 - \cos \alpha) \quad (6)$$

As with the bias, the local relative error does not converge asymptotically to zero when α is non-zero:

$$\lambda \rightarrow \infty, \text{LRE}_{D\infty d} \rightarrow -(1 - \cos \alpha) \tag{7}$$

This analysis suggests that some improvements can be obtained by varying the effective flow width (w) according to the flow direction as follows:

$$w = d \cos(\alpha) \tag{8}$$

The computed SCA is then equal to:

$$a_C = \frac{(l + 0.5)d}{d \cos \alpha} = \frac{\mu}{\cos \alpha} d \tag{9}$$

In the following we call this approach $D\infty v$. The difference between the two methods ($D\infty d$ and $D\infty v$) is null for $\alpha = 0$ and maximum for $\alpha = \pi/4$. For the $D\infty v$ method the bias on a strip of pixel along the direction y is:

$$\text{BIAS}_{D\infty v}(\rho, \alpha) = \frac{L}{2\rho \cos \alpha} \tag{10}$$

which then does converge to zero with increasing plane resolution, for all α . It can also be shown that:

$$|\text{BIAS}_{D\infty v}| < |\text{BIAS}_{D\infty d}| \quad \text{for } \rho > \frac{1 + \cos \alpha}{1 - \cos \alpha} \tag{11}$$

The local relative error can be expressed as a function of the upslope area resolution and the flow direction as follows:

$$\text{LRE}_{D\infty v} = \frac{1}{2\lambda \cos \alpha} \tag{12}$$

It can also be shown that:

$$|\text{LRE}_{D\infty v}| < |\text{LRE}_{D\infty d}| \quad \text{for } \lambda > \frac{1 + \cos \alpha}{(1 - \cos \alpha) \cos \alpha} \tag{13}$$

Therefore, the computation of the SCA with $D\infty$ can be improved by varying the flow width according to the local flow direction ($D\infty v$ method) on plane slopes, at least above certain resolution thresholds. These resolution thresholds decrease as α increases from 0 to $\pi/4$. The smallest values are $\rho = 6$ and $\lambda = 8.3$ for $\alpha = \pi/4$.

Planar slope—D8

D8 assumes that the flow can only be oriented along a single cardinal or diagonal direction, following the steepest descent to the nearest neighbouring pixels. Slope to a neighbouring downslope pixel is computed as the ratio of the difference in elevation to the relative planar distance of the corresponding pixel centres. The distance is therefore equal to d between pixels along the cardinal direction, while it is equal to $\sqrt{2}d$ between pixels along the diagonal direction. If the descent to adjacent cells is the same, then the downslope cell is selected arbitrarily among these or, particularly in flat regions, by carrying out the analysis on an enlarged neighbourhood, until a steepest descent is found (Jenson and Domingue, 1998).

On planar slopes, D8 computes the flow direction correctly only when $\alpha = 0$ and $\alpha = \pi/4$. For $0 \leq \alpha \leq \pi/8$, the computed flow direction is equal to 0, while for $\pi/8 \leq \alpha \leq \pi/4$, the flow direction is equal to $\alpha = \pi/4$. For $\alpha = \pi/8$, the flow direction is not unequivocally defined on a plane.

As for $D\infty$, the computed TCA at the centre of a pixel located at a distance l from the top edge of the slope is $(l + 0.5)d$.

Two approaches have been reported in the literature for the definition of the flow width when computing SCA with D8. These are:

1. Flow width always equal to the grid size, as in Wolock and McCabe (1995) or Zhang and Montgomery (1994);
2. Flow width equal to the grid size when flow is oriented in the cardinal direction, and equal to the pixel diagonal when flow is oriented in the diagonal direction, as indicated in Costa-Cabral and Burges (1994) or Wilson and Gallant (2000).

In the following we call the first method D8_d and the second method D8_v1. On a sloping plane as in Figure 2, D8_d gives the same results as D ∞ d, and equations (3) to (7) apply also to D8_d. D8_v1 changes the flow width to $\sqrt{2}d$ when the computed flow direction is diagonal. Therefore, the SCA results are:

$$\begin{aligned} a_C(\mu, \alpha) &= \mu d & 0 \leq \alpha \leq \pi/8 \\ a_C(\mu, \alpha) &= \mu \frac{d}{\sqrt{2}} & \pi/8 \leq \alpha \leq \pi/4 \end{aligned} \quad (14)$$

Thus, equations (3) to (7) apply also to D8_v1 if $0 \leq \alpha \leq \pi/8$. For $\pi/8 \leq \alpha \leq \pi/4$, the bias on a strip of pixels along the direction y is:

$$\text{BIAS}_{\text{D8}_v1}(\rho, \pi/8 \leq \alpha \leq \pi/4) = \frac{L}{2\sqrt{2}\rho \cos \alpha} [\sqrt{2} - (1 + \rho)(\sqrt{2} - \cos \alpha)] \quad (15)$$

The local relative error for a generic pixel with upslope catchment resolution λ is:

$$\text{LRE}_{\text{D8}_v1}(\lambda, \pi/8 \leq \alpha \leq \pi/4) = \frac{1}{2\sqrt{2}\lambda} - \left(1 - \frac{\cos \alpha}{\sqrt{2}}\right) \quad (16)$$

If plane resolution is progressively increased, both the bias and the local relative error do not converge asymptotically to zero, in particular:

$$\rho \rightarrow \infty, \text{BIAS}_{\text{D8}_v1}(\rho, \pi/8 \leq \alpha \leq \pi/4) \rightarrow -L \frac{\sqrt{2} - \cos \alpha}{2\sqrt{2} \cos \alpha} \quad (17)$$

$$\rho \rightarrow \infty, \text{LRE}_{\text{D8}_v1}(\lambda, \pi/8 \leq \alpha \leq \pi/4) \rightarrow -\left(1 - \frac{\cos \alpha}{\sqrt{2}}\right) \quad (18)$$

It can be shown that $|\text{BIAS}_{\text{D8}_v1}(\rho, \pi/8 \leq \alpha \leq \pi/4)| < |\text{BIAS}_{\text{D8}_d}(\rho, \pi/8 \leq \alpha \leq \pi/4)|$ only for low resolutions and in particular in the following three cases: $\rho = 1$; $\rho = 2$ and $\alpha < 0.66$ rad; $\rho = 3$ and $\alpha < 0.48$ rad. It can also be shown that $|\text{LRE}_{\text{D8}_v1}(\rho, \pi/8 \leq \alpha \leq \pi/4)| < |\text{LRE}_{\text{D8}_d}(\rho, \pi/8 \leq \alpha \leq \pi/4)|$ only for low upslope area resolutions, decreasing from 2 to 1 as α increases from $\pi/8$ to $\pi/4$.

Now we assess whether improvements could be achieved by assuming flow width equal to $d/\sqrt{2}$ for $\pi/8 \leq \alpha \leq \pi/4$, as suggested by Equation (8). We call this method D8_v2. In this case, bias and local error are given by the following relations:

$$\text{BIAS}_{\text{D8}_v2}(\rho, \pi/8 \leq \alpha \leq \pi/4) = \frac{L}{2\rho \cos \alpha} [1 - (1 + \rho)(1 - \sqrt{2} \cos \alpha)] \quad (19)$$

$$\text{LRE}_{\text{D8}_v2}(\lambda, \pi/8 \leq \alpha \leq \pi/4) = \frac{1}{\sqrt{2}\lambda} - (1 - \sqrt{2} \cos \alpha) \quad (20)$$

It can be shown that, compared to D8_d, the bias of D8_v2 is lower than D8_d if:

$$\rho > 5 \quad \text{and} \quad \alpha > \arccos \left[\frac{2\rho}{(1 + \rho)(\sqrt{2} + 1)} \right] \quad (21)$$

The interval of flow directions defined by Equation (21) becomes significant (larger than one-third of the interval $\pi/8 \leq \alpha \leq \pi/4$) only for $\rho > 15$.

The local relative error of the D8_v2 method is lower than D8_d if:

$$\lambda > \frac{\sqrt{2} + 1}{2[2 - (1 + \sqrt{2}) \cos \alpha]} \quad \text{and} \quad \alpha > \arccos\left(\frac{2}{\sqrt{2} + 1}\right) \cong 0.59 \text{ rad} \quad (22)$$

This threshold value for λ increases from 4.2 to infinity as α increases from 0.59 to 0.78 radians. Ultimately, compared to D8_d, D8_v2 gives the best results for high spatial resolutions, while D8_v1 only for very low spatial resolutions. The differences among the three analysed methods are maximum for $\alpha = \pi/4$.

INWARD CONES

We use the following rules in gridding cones (see Figure 3): the peak of the cone is located at a pixel corner, and pixels are part of the cone surface if pixel centres are located at a distance from the centre less than the cone radius. The cone can be either an inward cone (like a circular crater) or an outward cone (like a circular mountain). In this section we analyse the case of the inward cone.

The characteristic dimension L of the cone is the radius. The ratio $\rho = L/d$ represents the ‘cone resolution’. The theoretical SCA at a generic point of the inward cone located at a distance r from the centre is equal to:

$$a_T = \frac{L^2 - r^2}{2r} \quad (23)$$

The resolution of the upslope surface area is defined as the ratio of the theoretical specific upslope area, representing the extent of the upslope area, to the grid size and is a function of the cone resolution and the ratio of the distance from the pixel centre and the rim of the cone to the grid size (μ):

$$\lambda = \frac{a_T}{d} = \frac{\rho^2 - \mu^2}{2\mu} \quad (24)$$

In the following we compare the theoretical SCA pattern with those computed using the D ∞ and D8 algorithms, accounting for the cone resolution and the patterns of the upslope area resolution.

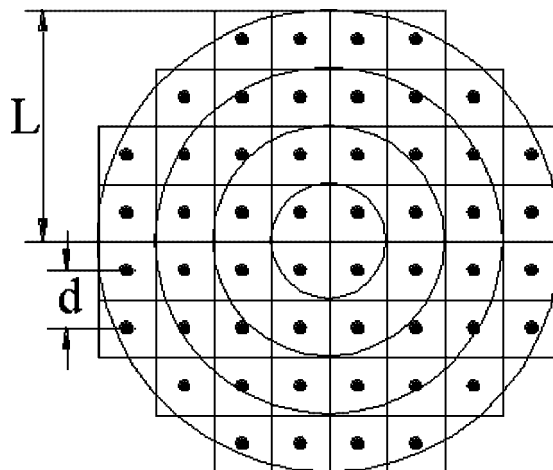


Figure 3. Grid representation of a circular cone

Inward cones— D_{∞}

While analysing the case of the sloping planes, we discussed two different approaches for the computation of the flow widths when computing SCA with the D_{∞} algorithm. These are:

1. $D_{\infty d}$, flow width always equal to the grid size independently of pixel flow direction;
2. $D_{\infty v}$, flow width varying with the flow direction as in Equation (8).

The second approach has been designed by analysing the properties of the TCA patterns on sloping planes according to different flow direction. Here we evaluate the two approaches on inward cones. For the D_{∞} approach, the angle α of Equation (8) is taken as the angle between the flow direction (as computed by D_{∞}) and the closest cardinal direction. The two approaches are evaluated by comparing the computed SCA patterns to the theoretical values defined by Equation (23), considering different cone resolutions. The following error statistics have been computed on cones with a radius of 100 units, represented by 11 different cone resolutions, ranging from 8 to 100, i.e. grid size between 12.5 units and 1 unit:

$$\text{absolute bias ABIAS} = \left| \sum (a_{Ci} - a_{Ti}) \right| / N \quad (25)$$

$$\text{mean absolute error MAE} = \sum |a_{Ci} - a_{Ti}| / N \quad (26)$$

The four pixels at the centre of the cone are excluded from the computation of these statistics because D_{∞} cannot compute the flow direction for elements with no downslope neighbours. The error statistics are plotted in Figure 4. By varying the flow width with the flow direction as in Equation (8), the bias becomes smaller for cone resolutions larger than 20, while the mean absolute error becomes smaller for cone resolutions larger than 8. As in the case of the sloping planes, the absolute bias of $D_{\infty d}$ does not converge to zero for increasing resolutions, whereas $D_{\infty v}$ does.

It is also interesting to look at the patterns of the local relative error as a function of the upslope catchment resolution (λ). Points with lower upslope catchment resolution correspond to pixels where the relative error is likely to be affected more by the poorer grid discretization of the upslope area, rather than to the actual

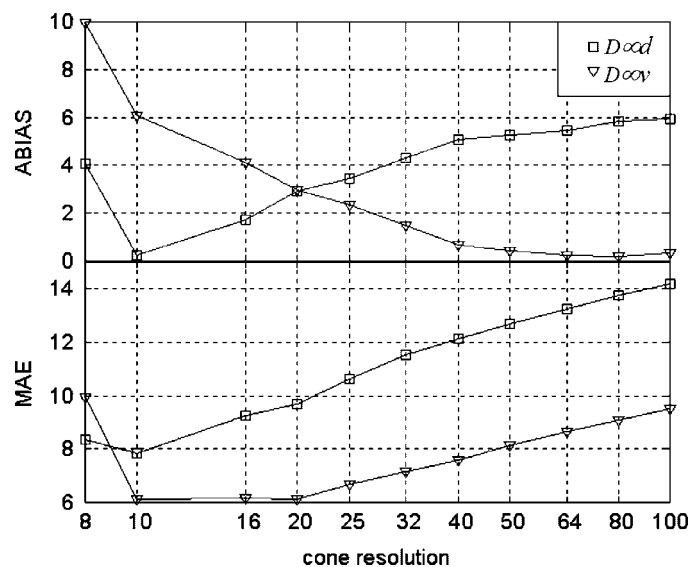


Figure 4. Error statistics of the SCA patterns computed on an inward cone with: (1) $D_{\infty d}$ and (2) $D_{\infty v}$. The cone resolution is expressed in logarithmic scale

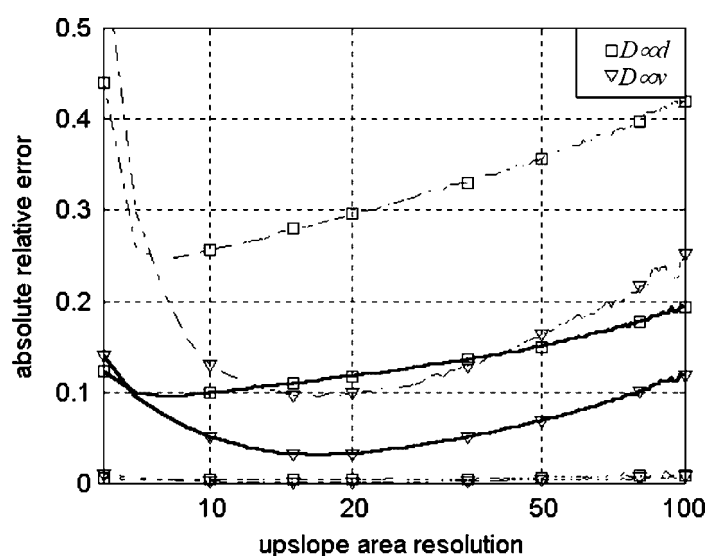


Figure 5. Absolute relative error of the SCA patterns computed on an inward cone with: (1) $D_{\infty d}$ and (2) $D_{\infty v}$. The continuous line describes the moving average on a centred window 10 units large. The broken lines represent the corresponding 0.025 and 0.975 percentiles. The upslope area resolution is in logarithmic scale

algorithm used to compute flow directions, upslope catchment area and flow width. The error values vary randomly while λ varies continuously within the range analysed. Therefore, in order to get a more robust estimate of the error trends versus λ , we calculated the average error statistics for all pixels within a range of $\lambda \pm 5$. Figure 5 shows these averaged errors plotted against λ . These averages can include values from all the different resolution grids, because points with the same upslope catchment resolution can represent points located at different distances from the border for different cone resolutions. Figure 5 also shows the values corresponding to the 0.025 and 0.975 percentiles of the absolute relative error in the centred moving window. $D_{\infty v}$ produces better average results for upslope area resolutions larger than 7, with a dispersion of the error around the average that is about half that of $D_{\infty d}$.

Inward cones—D8

We compare the SCA patterns computed on inward cones with the D8 algorithm, using the three different definitions of flow width that have been discussed while analysing the sloping plane. These are:

1. D8_d, flow width always equal to the grid size;
2. D8_v1, flow width changed to $\sqrt{2}$ times the grid size when the computed flow direction is diagonal;
3. D8_v2, flow width changed to $1/\sqrt{2}$ times the grid size when the computed flow direction is diagonal.

The analysed cone radius and resolutions are the same as those presented in the previous section. Again the methods are evaluated by comparing absolute bias (ABIAS, Equation (25)) and mean absolute error (MAE, Equation (26)) versus the cone resolution and the patterns of absolute relative error versus the upslope area resolution. For the same reasons given for D_{∞} , the four pixels located at the centre of the cones are excluded while computing the error statistics. The results are illustrated in Figures 6 and 7. In terms of absolute bias, D8_d produces the best results for cone resolutions between 10 and 40. For larger resolutions D8_v2 gives the best results. In terms of mean absolute error, differences between D8_v1 and D8_d are not significant. D8_v1 produces slightly better results for cone resolution smaller than 16. The mean absolute error of D8_v2 is larger than D8_d for cone resolutions smaller than 40, while it is similar to D8_d for larger cone resolutions. It is

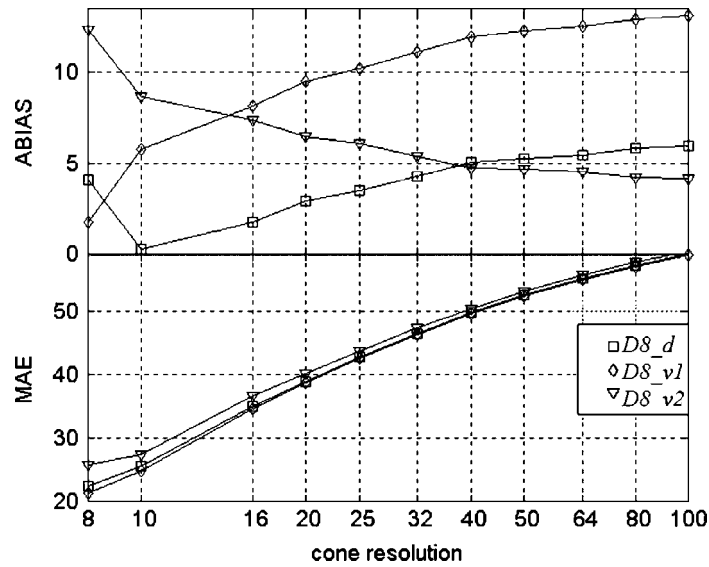


Figure 6. Error statistics of the SCA patterns computed on an inward cone with: (1) D8_d, (2) D8_v1 and (3) D8_v2. The cone resolution is expressed in logarithmic scale

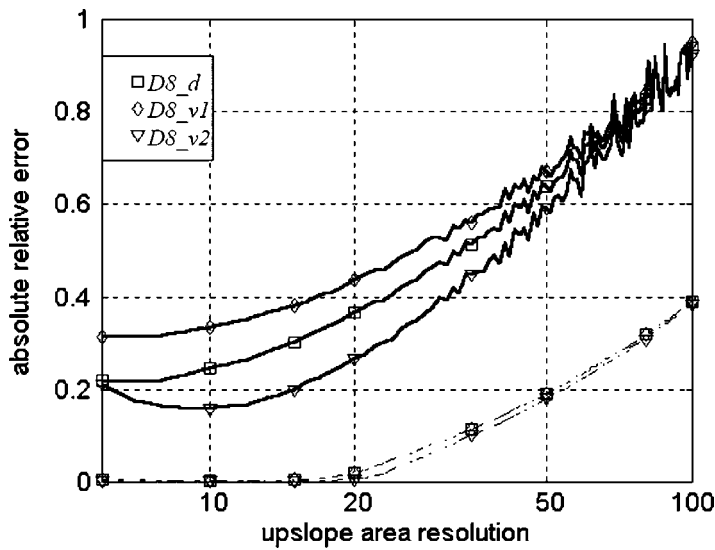


Figure 7. Absolute relative error of the SCA patterns computed on an inward cone with: (1) D8_d, (2) D8_v1 and (3) D8_v2. The continuous line describes the moving average on a centred window 10 units large. The broken lines represent the corresponding 0-025 percentiles. The upslope area resolution is in logarithmic scale

interesting to note that D8_d gives an absolute bias very close to $D\infty$ on inward cones. D8_v2 also produces better results in terms of average relative absolute error versus upslope catchment resolution, although with a larger dispersion towards larger values (Figure 8), while D8_v1 always produces the worst results.

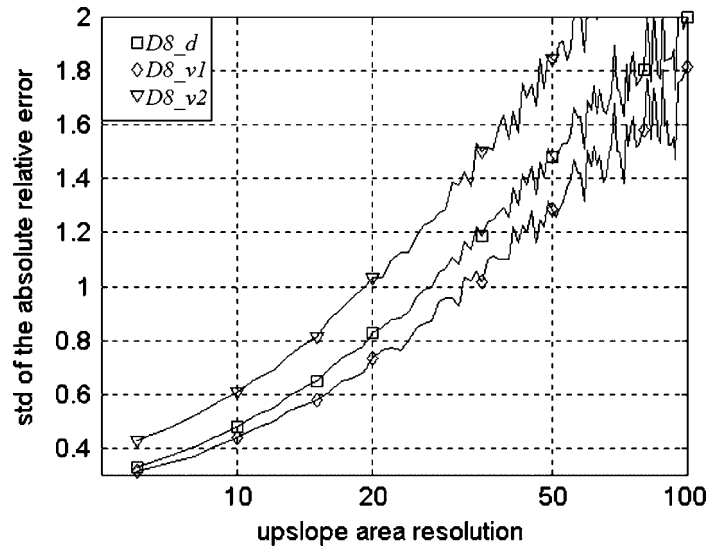


Figure 8. Standard deviation (std) of the absolute relative error of the SCA patterns computed on an inward cone with: (1) D8_d, (2) D8_v1 and (3) D8_v2. The std has been computed on a centred window 10 units large. The upslope area resolution is in logarithmic scale

OUTWARD CONE

The outward cone is discretized following the same rules used in the case of the inward cone, as depicted in Figure 3. The theoretical SCA in a generic point of the outward cone located at a distance r from the centre is:

$$a_T = \frac{r}{2} \tag{27}$$

The resolution of the upslope surface area is therefore a function only of the ratio of the distance of the pixel centre from the point of the cone to the grid size (μ):

$$\lambda = \frac{a_T}{d} = \frac{\mu}{2} \tag{28}$$

Now we compare the theoretical SCA pattern with those computed using the $D\infty$ and D8 algorithms, accounting for the cone resolution and the patterns of the upslope catchment resolution.

Outward cone— $D\infty$

As for the case of the inward cone, we evaluate the two methods, $D\infty d$ and $D\infty v$, by comparing the computed patterns to the theoretical patterns. Figure 9 shows the absolute bias (ABIAS, Equation (25)) and the mean absolute error (MAE, Equation (26)) versus the cone resolution. $D\infty v$ gives better results for resolutions larger than 25 with respect to both statistics. Again the ABIAS of $D\infty d$ does not converge to zero for increasing resolutions, while $D\infty v$ does. In terms of average absolute relative error, $D\infty v$ produces better results for upslope resolutions larger than 10, although the differences are small (Figure 10). $D\infty d$ produces patterns of absolute relative error that converge to a non-zero uniform value for a large upslope area resolution, as for the sloping plane.

Outward cone—D8

We evaluate the three methods D8_d, D8_v1 and D8_v2 by comparing absolute bias (ABIAS, Equation (25)) and mean absolute error (MAE, Equation (26)) versus the cone resolution and the patterns of absolute relative

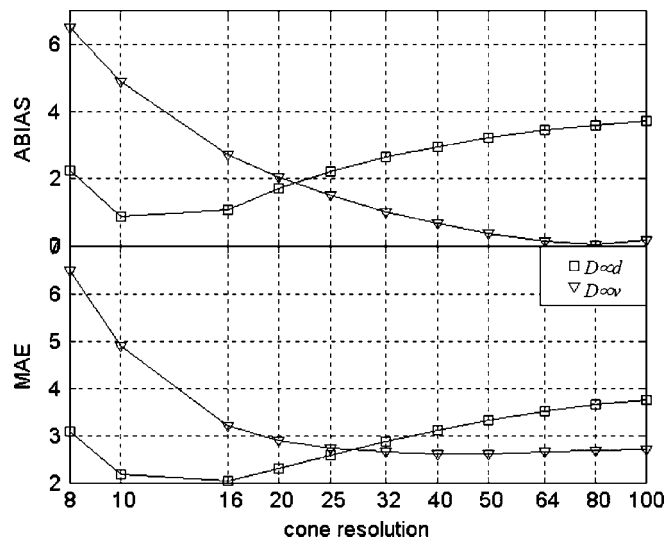


Figure 9. Error statistics of the SCA patterns computed on an outward cone with: (1) $D_{\infty d}$ and (2) $D_{\infty v}$. The cone resolution is expressed in logarithmic scale

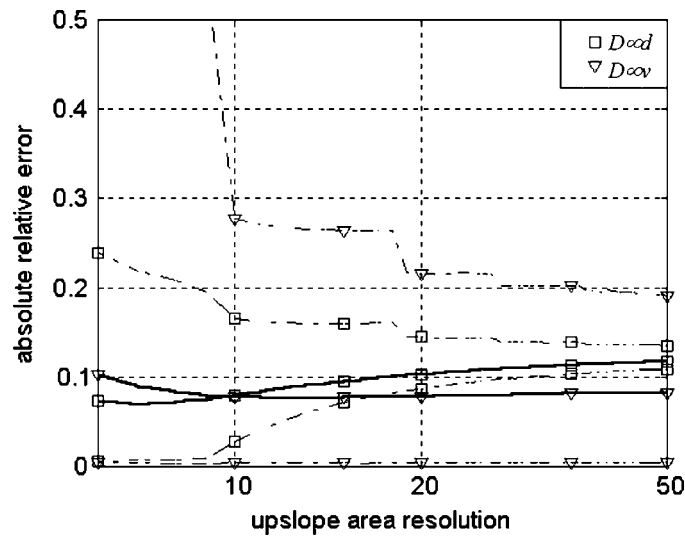


Figure 10. Absolute relative error of the SCA patterns computed on an outward cone with: (1) $D_{\infty d}$ and (2) $D_{\infty v}$. The continuous line describes the moving average on a centred window 10 units large. The broken lines represent the corresponding 0.025 and 0.975 percentiles. The upslope area resolution is in logarithmic scale

error versus the upslope area resolution. As shown in Figure 11, $D8_v2$ produces patterns with lowest absolute bias for cone resolutions larger than 25. We also verified that $D8_v1$ produces the lowest absolute bias only for global resolutions less than 7, while the lowest mean absolute error for global resolutions less than 6 (not shown in Figure 11). The absolute relative error is not sensitive to the upslope area resolution (see Figure 12). The differences between the three methods are small both in terms of average values and error dispersions. $D8_d$ still produces slightly better results.

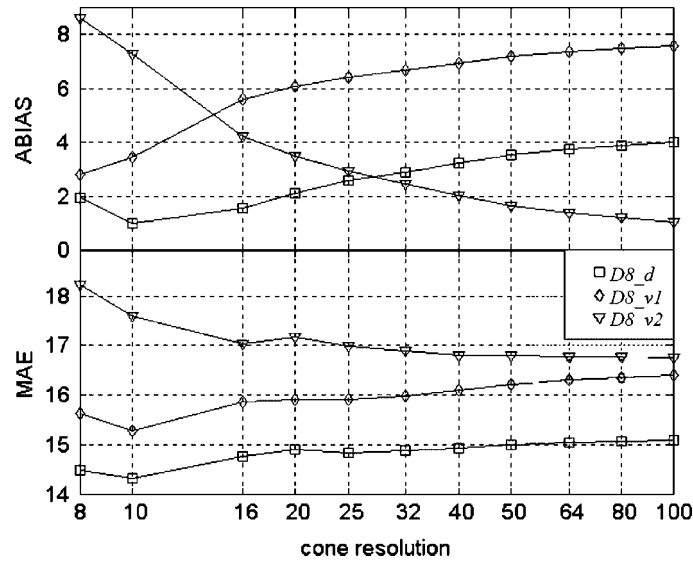


Figure 11. Error statistics of the SCA patterns computed on an inward cone with: (1) D8_d, (2) D8_v1 and (3) D8_v2. The cone resolution is expressed in logarithmic scale

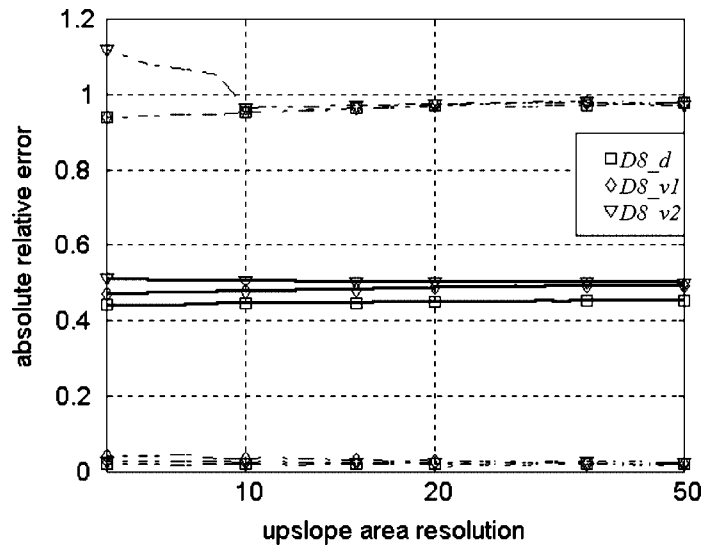


Figure 12. Absolute relative error of the SCA patterns computed on an inward cone with: (1) D8_d, (2) D8_v1 and (3) D8_v2. The continuous line describes the moving average on a centred window 10 units large. The broken lines represent the corresponding 0.025 and 0.975 percentiles. The upslope area resolution is in logarithmic scale

DISCUSSION AND CONCLUSIONS

We evaluated different methods for defining the flow width on grids, when computing the specific catchment area patterns using the D_{∞} and D8 algorithms. The analysis was conducted on sloping planes, inward and outward cones, and the results were compared with the theoretical SCA.

For a given DEM grid size, the error of the computed SCA in a pixel is related partly to the approximations of the applied algorithm and partly to the quality of the grid representation of the upslope area. Therefore we

identified two dimensionless parameters to evaluate the performance of the different methods:

1. Global resolution, defined as the ratio of a characteristic length of the study area to the grid size;
2. Upslope area resolution, defined as the ratio of the local theoretical SCA to the grid size.

The first is used to describe the bias and the mean absolute error across the entire area for different grid sizes. The second is used to describe the patterns of relative error for different grid sizes. In particular, the performance in relative error is analysed by comparing the values of pixels with similar upslope area resolution, as the errors in pixels with similar upslope area resolution are likely to be more evenly affected by the quality of the gridded representation of the upslope area. We discussed two methods for defining the flow width when using D_{∞} :

1. Flow width always equal to the grid size independently of pixel flow direction ($D_{\infty d}$ method);
2. Flow width varying as a function of the flow direction, as described in Equation (8) ($D_{\infty v}$ method).

We also compared three methods for defining the flow width when using D_8 :

1. Flow width always equal to the grid size independently of pixel flow direction (D_{8d} method);
2. Flow width equal to the grid size for cardinal flow directions and the grid size times $\sqrt{2}$ when the computed flow direction is diagonal (D_{8v1} method);
3. Flow width equal to the grid size for cardinal flow directions and the grid size times $1/\sqrt{2}$ when the computed flow direction is diagonal (D_{8v2} method).

We derived the $D_{\infty v}$ and D_{8v2} methods by analysing the properties of the computed total catchment area and flow directions on sloping planes. Table I illustrates the intervals of global and relative resolution thresholds for which $D_{\infty v}$ performs better than $D_{\infty d}$ for the different error statistics analysed, on sloping planes with flow direction at $\pi/4$ radians, and inward and outward cones. Similarly, Table II illustrates the intervals of global and relative resolution thresholds for which D_{8v1} and D_{8v2} perform better than D_{8d} . It is important to note that the differences between the analysed error statistics are more significant on planes with flow direction at $\pi/4$ radians than on inward or outward cones with similar characteristic lengths L (see Figures 2 and 3).

Compared with $D_{\infty d}$, $D_{\infty v}$ produces the lowest bias and mean absolute error when global resolution is larger than 25. It also performs better in terms of local relative error for local upslope area resolutions larger than 10. These resolution thresholds are quite high for most practical applications. Considering that average hillslope length is 150 m (McMaster, 2002; Tarboton *et al.*, 1991) and typical grid DEM sizes are from 25 m to 50 m, in practical applications the global resolution ρ of individual hillslopes is around 3–6, while local upslope area resolutions are on average less than 6. Therefore, when SCA patterns are computed with D_{∞} , changing the flow width according to the flow direction, as suggested by Equation (8), is preferable only if

Table I. Intervals of global (ρ) and relative resolution (λ) for which the $D_{\infty v}$ method has been verified to perform better than the $D_{\infty d}$ method, for different error statistics (ABIAS = absolute bias, MAE = mean absolute error, LRE = absolute local relative error)

	Plane ($\alpha = \pi/4$ rad)	Inward cone	Outward cone
ABIAS	$\rho > 5$	$\rho > 20$	$\rho > 20$
MAE	$\rho > 5$	$\rho > 8$	$\rho > 25$
LRE	$\lambda > 8$	$\lambda > 7$	$\lambda > 10$

Table II. Intervals of global (ρ) and relative resolution (λ) for which D8_v1 and D8_v2 methods have been verified to perform better than or similarly to the D ∞ d method, for different error statistics (ABIAS = absolute bias, MAE = mean absolute error, LRE = local relative error)

		Plane ($\alpha = \pi/4$ rad)	Inward cone	Outward cone
D8v1	ABIAS	$\rho < 2$	$\rho < 10$	$\rho < 7$
	MAE	$\rho < 2$	$\rho < 16$	$\rho < 6$
	LRE	$\lambda = 1$	never	never
D8v2	ABIAS	$\rho > 5$	$\rho > 40$	$\rho > 25$
	MAE	$\rho > 5$	similar for $\rho > 40$	never
	LRE	$\lambda > 4$	any λ	never

very high DEM resolutions are employed, i.e. grid DEM sizes of 5 m or less. In all other cases, it is better to assume the flow width invariant and equal to the grid size.

D8_v1 performs significantly better than D8_d in terms of ABIAS and MAE only for low global resolution thresholds, particularly on sloping planes. These resolution thresholds are lower than those employed in most practical circumstances. In terms of LRE, the performance of D8_v1 is always worse than D8_d.

D8_v2 performs significantly better than D8_d on sloping planes only for high global and local upslope area resolution thresholds, larger than those employed in practical circumstances. Its performance is also better on inward cones in terms of local relative error. In all other circumstances analysed, the results of D8_v2 are generally poorer than or similar to those obtained with D8_d.

Therefore, changing the flow width according to the local flow direction using the D8_v1 method is not only conceptually wrong but leads to poorer results than the D8_d method. Also, the D8_d method performs better than the alternative D8_v2 method that we defined by analysing the total catchment area and flow directions computed with D8 on sloping planes, at least for the DEM resolutions normally employed.

In summary, assuming an invariant flow width equal to the grid size is the best approach when SCA are computed with the D8 and D ∞ algorithms in most practical circumstances (i.e. unless a very high resolution DEM is available).

REFERENCES

- Beven KJ, Kirkby MJ. 1979. A physically based, variable contributing area model of basin hydrology. *Hydrological Sciences Bulletin* **24**: 43–69.
- Costa-Cabral MC, Burges SJ. 1994. Digital Elevation Model Networks (DEMON)—a model of flow over hillslopes for computation of contributing and dispersal areas. *Water Resources Research* **30**(6): 1681–1692.
- Dietrich WE, Wilson CJ, Montgomery DR, McKean J. 1993. Analysis of erosion threshold, channel networks, and landscape morphology using digital terrain model. *Journal of Geology* **20**: 675–679.
- Fairfield J, Leymarie P. 1991. Drainage networks from digital elevation models. *Water Resources Research* **27**(5): 709–717.
- Freeman TG. 1991. Calculating catchment area with divergent flow based on a regular grid. *Computers and Geosciences* **17**(3): 413–422.
- Gallant JC, Wilson JP. 2000. Primary topographic attributes. In *Terrain Analysis: Principles and Applications*, Wilson JP, Gallant JC (eds). Wiley: New York; 51–85.
- Jenson S, Domingue J. 1988. Extracting topographic structure from digital elevation data. *Photogrammetric Engineering and Remote Sensing* **54**(11): 1593–1600.
- Lea NL. 1992. An aspect driven kinematic routing algorithm. In *Overland Flow: Hydraulics and Erosion Mechanics*, Parsons AJ, Abrahams AD (eds). Chapman & Hall: New York.
- Maunder CJ. 1999. An automated method for constructing contour-based digital elevation models. *Water Resources Research* **35**(12): 3931–3940.
- McMaster KJ. 2002. Effects of digital elevation model resolution on derived stream network positions. *Water Resources Research* **38**(4): 1042.
- Montgomery DR, Dietrich WE. 1994. A physically-based model for the topographic control on shallow landsliding. *Water Resources Research* **30**(4): 1153–1171.
- Moore ID, Grayson RB, Ladson AR. 1991. Digital Terrain Modeling—a review of hydrological, geomorphological, and biological applications. *Hydrological Processes* **5**(1): 3–30.

- O'Callaghan JF, Mark DM. 1984. The extraction of drainage networks from digital elevation data. *Computer Vision, Graphics and Image Processing* **28**: 323–344.
- O'Loughlin EM. 1981. Saturation regions in catchment and their relations to soil and topographic properties. *Journal of Hydrology* **53**: 229–246.
- Pack RT, Tarboton DG, Goodwin CN. 1998. The SINMAP approach to terrain stability mapping. *8th Congress of the International Association of Engineering Geology*, Vancouver, BC, Canada.
- Quinn P, Beven K, Chevallier P, Planchon O. 1991. The prediction of hillslope flow paths for distributed hydrological modelling using digital terrain models. *Hydrological Processes* **5**: 59–80.
- Quinn PF, Beven KJ, Lamb R. 1995. The $\text{Ln}(a/\text{Tan-Beta})$ index—how to calculate it and how to use it within the TOPMODEL framework. *Hydrological Processes* **9**(2): 161–182.
- Tarboton DG. 1997. A new method for the determination of flow directions and upslope areas in grid digital elevation models. *Water Resources Research* **33**(2): 309–319.
- Tarboton D, Bras R, Rodriguez-Iturbe I. 1991. On the extraction of channel networks from digital elevation data. *Hydrological Processes* **5**: 81–100.
- Wolock DM, McCabe JJ. 1995. Comparison of single and multiple flow direction algorithms for computing topographic parameters in TOPMODEL. *Water Resources Research* **31**: 1315–1324.
- Zhang W, Montgomery DR. 1994. Digital elevation model grid size, landscape representation and hydrologic simulations. *Water Resources Research* **30**(4): 1019–1028.